

UNAVOIDABLE SELECTION EFFECTS IN THE ANALYSIS OF FAINT GALAXIES IN THE HUBBLE DEEP FIELD: PROBING THE COSMOLOGY AND MERGER HISTORY OF GALAXIES

TOMONORI TOTANI¹ AND YUZURU YOSHII^{2,3}

To Appear in the Astrophysical Journal

ABSTRACT

We present a detailed analysis of the number count and photometric redshift distribution of faint galaxies in the Hubble Deep Field (HDF), paying a special attention to the selection effects including the cosmological dimming of surface brightness of galaxies, under the observational condition employed in this field. We find a considerably different result from previous studies ignoring the selection effects, and these effects should therefore be taken into account in the analysis. We find that the model of pure luminosity evolution (PLE) of galaxies in the Einstein-de Sitter (EdS) universe predicts much smaller counts than those observed at faint magnitude limits by a factor of more than 10, so that a very strong number evolution of galaxies with $\eta \gtrsim 3$ –4 must be invoked to reproduce the I_{814} counts, when parametrized as $\phi^* \propto (1+z)^\eta$. However we show that such a strong number evolution under realistic merging processes of galaxies can not explain the steep slope of the B_{450} and V_{606} counts, and it is seriously inconsistent with their photometric redshift distribution. We find that these difficulties still persist in an open universe with $\Omega_0 \gtrsim 0.2$, but are resolved only when we invoke a Λ -dominated flat universe, after examining various systematic uncertainties in modeling the formation and evolution of galaxies. The present analysis revitalizes the practice of using faint number counts as an important cosmological test, giving one of the arguments against the EdS universe and suggests acceleration of the cosmic expansion by vacuum energy density. While a modest number evolution of galaxies with $\eta \lesssim 1$ is still necessary even in a Λ -dominated universe, a stronger number evolution with $\eta > 1$ is rejected from the HDF data, giving a strong constraint on the merger history of galaxies.

Subject headings: cosmology: observations — galaxies: evolution — galaxies: formation

1. INTRODUCTION

Number counting of faint galaxies is one of the most fundamental observational tests with which the formation/evolution of galaxies as well as the geometry of the universe is probed. The best view to date of the optical sky to faint flux levels is given by the Hubble Deep Field (HDF, Williams et al. 1996), and it provides a valuable information to a wide range of studies on galaxies and cosmology. A comprehensive study of the HDF galaxy counts has been performed by Pozzetti et al. (1998), and they found that a simple model of pure luminosity evolution (PLE), in which galaxies evolve passively due to star formation histories without mergers or number evolution, gives a reasonable fit to the HDF counts in all the four passbands of U , B , V , and I , when an open universe with $\Omega_0 = 0.1$ is assumed.

The increase of the number of galaxies with their apparent magnitude was originally proposed as a measure of the geometry of the universe (Sandage 1961), and considerable efforts have been made along this line (e.g., Yoshii &

Takahara 1988; Fukugita, Takahara, Yamashita & Yoshii 1990; Yoshii & Peterson 1991). However, the obtained constraints on cosmological parameters based on the PLE model have not been thought deterministic because of possible number evolution of galaxies by mergers. Particularly, when the PLE model is used, the Einstein-de Sitter (EdS) universe ($\Omega_0 = 1$) underpredicts the observed galaxy counts at faint magnitudes, but a simple model of galaxy number evolution can reproduce the observed counts and save the EdS universe (Rocca-Volmerange & Guideroni 1990; Pozzetti et al. 1996). This degeneracy between the effects of galaxy evolution and cosmology has been a major problem when one uses the galaxy number count to determine the geometry of the universe.

The information of redshifts is able to break such a degeneracy, because luminous galaxies at great distance are distinguishable from dwarf galaxies in a local universe. Although most of the HDF galaxies are too faint to measure the spectroscopic redshifts, several catalogs of their

¹ National Astronomical Observatory, Mitaka, Tokyo 181-8588, Japan (E-mail: totani@th.nao.ac.jp)

²Institute of Astronomy, School of Science, The University of Tokyo, 2-21-1 Osawa, Mitaka, Tokyo 181-8588, Japan

³Research Center for the Early Universe, Faculty of Science, The University of Tokyo, Tokyo 113-0033, Japan

photometric redshifts have been published (Sawicki, Lin, & Yee 1997; Wang, Bahcall, & Turner 1998; Fernández-Soto, Lanzetta, & Yahil 1999). The follow-up studies based on these catalogs show that the photometric redshifts give reasonably reliable estimates of spectroscopic redshifts and are useful for a statistical study of the HDF galaxies. Here we give a combined analysis for the HDF counts and redshifts and constrain the cosmological parameters separately from the merger history of galaxies.

Both the number count of faint galaxies and their redshift distribution are significantly affected by the selection effects inherent in the method of detecting galaxies in faint surveys, but these important effects have been ignored in almost all previous studies except for Yoshii & Fukugita (1991) and Yoshii (1993). It is well known that the surface brightness of galaxies rapidly becomes dimmer with increasing redshift as $\propto (1+z)^{-4}$ (Tolman 1934), and this cosmological dimming makes many high-redshift galaxies remain undetected below the threshold value of surface brightness adopted in a galaxy survey (Pritchett & Kline 1981; Tyson 1984; Ellis, Sievers, & Perry 1984). The seeing or smoothing of an image furthermore lowers its surface brightness, and the photometry scheme used in a survey heavily affects a magnitude estimate of the faintest galaxies. Some observers apply corrections to raw counts of faint galaxies for those undetected, but it is in principle difficult and heavily model-dependent to estimate the number of undetected galaxies. Rather, the best way is to make theoretical predictions with the selection effects taken into account and then compare them directly to raw counts (Yoshii 1993).

This paper is the first analysis of the HDF galaxies in which the above selection bias against high-redshift galaxies is explicitly incorporated. We use a standard PLE model of galaxies including the effects of internal dust obscuration and intergalactic HI absorption. Number evolution of galaxies is also allowed for with simple modifications to the PLE model. Throughout this paper, we use the AB photometry system with the notation of U_{300} , B_{450} , V_{606} , and I_{814} (Williams et al. 1996). In §2, we present a detailed description for models of galaxy evolution and formulations to calculate galaxy counts and redshift distribution with the selection effects taken into account. Extensive calculations of number count predictions and comparison to the HDF counts are given in §3, checking in great detail the uncertainties arising from the prescribed properties of local galaxies and their evolution. We will give the comparison of the model predictions with the observed photometric redshift distribution in §4. We discuss the results in §5. The summary and conclusion of this paper are given in §6.

2. THE MODEL OF GALAXIES AND DETECTION IN THE HDF

First we describe the basic ingredients involved in our theoretical modeling such as the local luminosity function, galaxy evolution in luminosity and number, internal and intergalactic absorption, and the selection effects. Then we will present the formulations to calculate the number count of faint galaxies and their redshift distribution.

2.1. Galaxies at Present, and Their Evolution

We use a standard PLE model of galaxy evolution, in which galaxies are classified into five morphological types of E/S0, Sab, Sbc, Scd, and Sdm. Spectral energy distributions (SEDs) and their evolution are calculated by using the galaxy evolution model of Arimoto & Yoshii (1987) for elliptical galaxies and the I1 model of Arimoto, Yoshii, & Takahara (1992) for spiral galaxies. These models are constructed to reproduce the photometric and chemical properties of present-day galaxies. In order to see the systematic uncertainty in evolution models, we will also use an updated version of these models by Kobayashi et al. (1999) using the latest database of stellar populations compiled by Kodama & Arimoto (1997). We set the epoch of galaxy formation at $z_F = 5$ as a standard and change this value to see the systematic uncertainty.

The luminosity function of local galaxies is also important in predicting the number count and redshift distribution of faint galaxies. We use the type-dependent (E/S0, Spiral, and Irr) B -band luminosity function derived from the Second Southern Sky Redshift Survey (SSRS2, Marzke et al. 1998). We associate the Sab, Sbc and Scd models to be assigned to spiral galaxies, whereas the Sdm model assigned to irregular galaxies. The relative proportions of Sab, Sbc, and Scd are taken from Pence (1976). In order to check the systematic uncertainty related to the luminosity function, we also use the type-independent luminosity function of Stromlo-APM redshift survey (Loveday et al. 1992) and the type-dependent luminosity function from the Center for Astrophysics (CfA) redshift survey (Huchra et al. 1983). Their Schechter parameters are tabulated in Table 1 (see also Efstathiou, Ellis, & Peterson 1988 and Yoshii & Takahara 1989).

2.2. Absorption

The above models of galaxy evolution do not include the absorption by interstellar dust which becomes significant for high- z galaxies when observed in optical bands. In order to take this effect into account, we make a physically natural assumption that the dust optical depth is proportional to the column density and metallicity of the gas. In fact, it is well known that the Galactic extinction is well correlated to the column density of the HI gas (e.g., Burstein & Heiles 1982). It is also known that the dust opacity becomes smaller in order of decreasing metallicity from the Galaxy to the Large and then Small Magellanic Clouds, when the gas column density is fixed (e.g., Pei 1992). Since the galaxy evolution models give the gas

fraction f_g and the metallicity Z_g in the gas, the dust optical depth is calculated from $\tau_{\text{dust}} = \kappa f_g Z_g r_e^{-2} (M/L_B) L_B$, where r_e , M , and L_B are the effective radius, the baryon mass, and the B -band luminosity of a galaxy, respectively. (We will describe the treatment of galaxy size in §2.3.) The proportionality constant κ is chosen to be consistent with the present-day, average extinction of $A_V \sim 0.17$ taken from the Galactic extinction map (Burstein & Heiles 1982; Schlegel, Finkbeiner, & Davis 1998) and a theoretical estimate (Hatano, Branch, & Deaton 1998). The standard extinction curve of our Galaxy (e.g., Pei 1992) is used for the wavelength dependence of the optical depth.

Given the optical depth, the attenuation of emerging stellar lights depends on the spatial dust distribution. Following Disney, Davies, & Phillipps (1989), there are two extreme cases such as the screen model in which the dust is distributed on the line of sight to stars, and the slab model in which the dust has the same distribution with stars. Neglecting the scattering of lights by dust, the attenuation factor of stellar lights is given by $\exp(-\tau_{\text{dust}})$ for the screen model and $[1 - \exp(-\tau_{\text{dust}})]/\tau_{\text{dust}}$ for the slab model. In fact, the galaxy evolution model used here has been made to reproduce the present-day SED of galaxies which has been already affected by dust obscuration. We take into account this point and hence correct the above attenuation factors by using the optical depth at present. Therefore the present-day SEDs of model galaxies are the same for all the prescriptions of dust-free, screen, and slab models.

In the slab model the apparent reddening reaches an asymptote when the optical depth becomes much larger than unity, because the observed lights are emitted from surface regions of a galaxy where the optical depth to an observer is low. However, the observed correlation between the power-law index of UV spectra and the Balmer line ratio, both of which are a reddening indicator, extends well beyond the asymptote. This indicates that the observed reddening of starburst galaxies is larger than expected from the slab model, and at least some fraction of dust should behave like a screen (for detail see Calzetti, Kinney, & Storchi-Bergmann 1994).

We then use the screen model as a standard, considering that UV and optical observations of starburst galaxies favor the screen dust. It may be an extreme prescription that all dust is distributed as a screen, but note that the emergent lights are rapidly attenuated exponentially once a considerable fraction of dust contributes to the screen. Therefore the screen model is more appropriate than the slab model in which the attenuation factor decreases only moderately like τ_{dust}^{-1} when $\tau_{\text{dust}} \rightarrow \infty$.

The spectral energy distributions (SEDs) of galaxies of various types are given in Fig. 1 at several epochs of galaxy evolution for three cases of dust extinction such as the screen model (solid line), the slab model (dashed line), and the no-extinction model (dotted line). The effect of

dust extinction is especially important for elliptical galaxies at high redshifts, where UV radiation is quite strong because of the initial starbursts supposed in the galactic wind model of elliptical galaxies (Arimoto & Yoshii 1987). According to the method described above, the dust optical depth during the initial starburst phase of elliptical galaxies is estimated to be much larger than unity ($\tau \gtrsim 10$) for UV photons at ~ 2000 Å in the restframe. On the other hand, the evolution of dust obscuration makes UV luminosity of late-type spiral galaxies brighter at early epochs than that without the dust effect, because of the lower metal abundance than the present-day galaxies. However, this effect in late-type spiral galaxies is not significant because they are not heavily obscured at present.

In addition to the internal absorption by dust, the intergalactic absorption significantly affects the visibility of high-redshift galaxies (Yoshii & Peterson 1994; Madau 1995). Lights from a distant galaxy at rest wavelengths below the Lyman limit (912 Å) and those below the Lyman α line (1216 Å) are extinguished by Lyman continuum absorption and Lyman series line absorption, respectively, in intergalactic HI clouds along the line of sight. We include this effect consistently in our theoretical calculations making use of the intergalactic optical depth calculated by Yoshii & Peterson (1994). The optical depth of this absorption is shown in Fig. 2, as a function of observed wavelength for various source redshifts.

2.3. Selection Effects

Apparent surface brightness and size of an image in a survey observation are the essential quantities for it to be detected as a real galaxy. We calculate these quantities of a model galaxy assuming its intrinsic luminosity profile and size and taking into account the cosmological dimming and the observational seeing. For the details of the formulations, see Yoshii (1993).

2.3.1. Galaxy Sizes and Luminosity Profile

In our PLE model, we assume that the galaxy size does not evolve except for the case of mergers of galaxies, and use the empirical relation between the effective radius r_e and absolute luminosity L_B for local galaxies. If we allow for the number evolution of galaxies, we must take into account the change of galaxy sizes, and we will discuss this in §2.4. Fig. 3 shows the size-luminosity relation of local elliptical and spiral galaxies. The data of elliptical galaxies are taken from Bender et al. (1992), and those of spiral galaxies from Impey et al. (1996). Although there is a significant scatter in this relation, we use a simple power-law relation for this relation as

$$r_e \propto L_B^{2.5/p}, \quad (1)$$

or, if expressed in terms of the absolute B magnitude,

$$-M_B = p \log r_e + q + (p-5) \log(H_0/50 \text{ km/s/Mpc}). \quad (2)$$

Elliptical galaxies form two distinct families which follow the well-separated sequences at low luminosities in the r_e - L_B diagram. One is the ordinary sequence from giant through dwarf elliptical (GDE) galaxies, while the other is the bright sequence from giant through compact elliptical (GCE) galaxies (see Fig 3). Since the predictions of galaxy number count are not sensitive to whichever sequence is used in the analysis (see §3.2 and Fig 9), we take the GDE sequence as the standard size-luminosity relation of elliptical galaxies in this paper.

The r_e - L_B relations fitted to the data in Fig.3 yield $(p, q) = (6.0, 16)$ and $(3.5, 18.7)$ for the GDE and GCE sequences of elliptical galaxies, respectively, and $(9.4, 12)$ for spiral galaxies. In order to examine the uncertainty due to the significant scatter in the r_e - L_B relation, we derive the standard deviation in $\Delta(\log r_e)$ from the best-fit relation and repeat calculations with the shifted relations shown in Fig. 3 by the dashed lines.

The radial distribution of surface brightness is assumed to follow de Vaucouleurs' (1962) profile ($S \propto \exp[-(r/r_e)^{1/4}]$) for elliptical galaxies and an exponential profile for spiral galaxies (Freeman 1970). Then we can calculate the radial distribution of surface brightness of a galaxy at given redshift in any passband, when the galaxy type, the present-day B luminosity, and the evolution model are specified. This surface brightness profile should be convolved with a Gaussian point-spread function (PSF) having the same dispersion with the observational seeing.

2.3.2. Object Detection

Let S_{th} be the surface brightness threshold adopted in a galaxy survey. Strictly, this threshold could change due to different noise levels within a survey field, but we use a single value for the simplicity. When the observed profile of a galaxy image is calculated as above, we can estimate the isophotal size which encircles a region of a galaxy image with surface brightness brighter than S_{th} . If the isophotal size of a galaxy is zero, i.e., the central surface brightness is fainter than S_{th} , this galaxy can not be detected in the survey. Usually a minimum isophotal diameter D_{min} , which is comparable to the seeing size, is adopted as a condition for an image to be detected as a galaxy. We can calculate the isophotal diameter for a model galaxy, then it is easy to check whether this galaxy meets the detection criterion in the galaxy survey.

2.3.3. Photometry Scheme

There are three photometry schemes to evaluate the apparent magnitude of galaxies such as isophotal, aperture, and pseudo-total magnitudes. These magnitudes may significantly differ especially near the detection limit, and this difference should be included in the theoretical modeling of the selection effects inherent in the method of detecting faint galaxies.

The isophotal magnitude is the flux within the isophotal size of a galaxy image. The aperture magnitude is the flux within a fixed aperture which is adopted by observers. Some observers often make corrections to these magnitudes into pseudo-total magnitudes, which are intended to mimic an ideal total flux of a galaxy. However, such corrections use a model luminosity profile to evaluate the flux from an ‘undetected’ part of a galaxy image. It is inappropriate to make a model-dependent correction to the observed quantities with which various theoretical models are compared. The best way is, on the contrary, to incorporate all the necessary corrections in the theoretical models to be compared directly with the observed quantities. We therefore suggest that observers should also present raw counts and magnitudes, in addition to presenting corrected quantities in their papers.

2.3.4. Detection and Photometry of the HDF Galaxies

Here we describe the detection processes of the HDF galaxies, following Williams et al. (1996), and see also Bouwens, Broadhurst, & Silk (1998). Object detection is performed in the combined $V_{606} + I_{814}$ image. It is first convolved with a fixed smoothing kernel of 25 pixels ($=0.04$ square arcseconds), then pixels having values higher than a fixed threshold above a local sky background are marked as potentially being part of an object. After thresholding, regions consisting of more than contiguous 25 pixels are counted as sources. It corresponds to an isophotal diameter limit of $D_{\text{min}} \sim 0.2$ arcsec, about 1.6 times larger than the FWHM of the PSF.

The surface brightness threshold is not clearly indicated in Williams et al. (1996), but we can evaluate this value from the surface brightness distribution of the HDF galaxies. In Fig. 4, we plot their apparent magnitudes versus average surface brightness in the four passbands of U_{300} , B_{450} , V_{606} , and I_{814} by using the published sizes and magnitudes of the HDF catalog. Here the size refers to the isophotal size of the combined $V_{606} + I_{814}$ image, and the magnitude refers to the isophotal magnitude measured within the isophotal size. First we consider the V_{606} and I_{814} bands. Figure 4 shows that no galaxies are detected when the average surface brightness is fainter than $S_{\text{th}} = 27.5 \text{ mag arcsec}^{-2}$ in V_{606} and $27.0 \text{ mag arcsec}^{-2}$ in I_{814} . The faintest surface brightness detected in the HDF for galaxies with a fixed isophotal magnitude becomes brighter for brighter galaxies. This trend occurs because the size of galaxies is larger for brighter galaxies. The edge of an isophotal image corresponds to the isophotal limit, and hence its average surface brightness within the isophotal area is always brighter than its threshold when the galaxy image have a bright central part and therefore a larger size. Consequently the faintest surface brightness

at the faintest isophotal magnitudes, i.e., $S_{\text{th}} = 27.5 \text{ mag arcsec}^{-2}$ in V_{606} and $27.0 \text{ mag arcsec}^{-2}$ in I_{814} , gives the surface brightness threshold for object detection. In our calculations the above threshold values in the V_{606} and I_{814} bands are used respectively, although in reality the detection was done by the combined $V_{606} + I_{814}$ image in the HDF catalog.

On the other hand, the surface brightness threshold is not clear in the U_{300} and B_{450} bands, because the object detection was done without these bands. It should also be noted that the isophotal U_{300} and B_{450} magnitudes are defined as the flux within the isophotal size in the combined $V_{606} + I_{814}$ image. Among the objects to which these isophotal magnitudes are assigned, those with $S/N > 2$ are detected as galaxy images in the U_{300} and B_{450} bands (Williams et al. 1996). We see a clear boundary indicated by dot-dashed line running from upper-left to lower-right in the U_{300} and B_{450} panels of Fig. 4, and this corresponds to the line of $S/N = 2$. It is easy to show that this is equivalent to a condition of $S + m = \text{const}$ if the noise level is proportional to $A^{1/2}$ (Poisson type noise), where A is the isophotal area. We have also confirmed that the galaxies in U_{300} and B_{450} with $S/N \sim 2$ are actually on the dot-dashed line of Fig. 4⁴. In our calculations the galaxies in the U_{300} and B_{450} bands are detected if they are detected in I_{814} band and furthermore meet the criterion of $S/N > 2$ within the isophotal area in the I_{814} band (i.e., those below the dot-dashed line in Fig. 4).

2.4. Merger and Number Evolution

Currently the most popular theory for the structure formation in the universe is the bottom-up scenario with the cold dark matter which dominates the total mass density of the universe, in which smaller mass objects form earlier and then merge into larger objects (e.g., Blumenthal et al. 1984). Merging history of dark matter haloes is relatively well studied by analytical methods as well as N -body simulations, but merging history of galaxies could significantly differ from that of dark matter haloes and is poorly known.

Since a number evolution of galaxies caused by galaxy mergers significantly affects the number count of faint galaxies, we investigate this effect by using a simple merging model in which the luminosity density of galaxies is conserved. A common practice for this is to introduce the redshift-dependent parameters of Schechter-type luminosity function of galaxies such as

$$\begin{aligned}\phi^*(z) &= \phi^*(0)(1+z)^\eta \\ L^*(z) &= L^*(0)(1+z)^{-\eta}.\end{aligned}\quad (3)$$

We adopt a single value of η for all types of galaxies for simplicity.

⁴This is true for the three WF fields, but not for the PC field, because of the different surface brightness threshold employed (Williams et al. 1996). The number of galaxies in the PC field is negligible compared with the WF fields.

In the analysis of this paper, the size of a galaxy is crucially important for evaluating the selection effects. Merger of galaxies should change their size, and this should also be taken into account. The empirical relation $r_e \propto L_B^{2.5/p}$ may not hold at high redshifts, depending on how r_e and L_B change during the merger process. We assume that the change of L_B and r_e during merger processes always satisfy a relation $L_B \propto r_e^\xi$. (Note that this relation is physically different from equation 1 which is the relation of galaxies at a fixed time, but describing the change of luminosity and size of a test galaxy during merger processes.) If $\xi = 2$, the surface brightness of galaxies is conserved during mergers, and if $\xi = 3$, the luminosity density in each galaxy is conserved. Then the luminosity and size of a $z = 0$ galaxy evolve as

$$L_B \rightarrow L_B(1+z)^{-\eta} \quad (4)$$

$$r_e \rightarrow r_e(1+z)^{-\eta/\xi}. \quad (5)$$

By applying this transformation to the empirical r_e - L_B relation at $z = 0$, it is straightforward to give the r_e - L_B relation as a function of redshift:

$$r_e(L_B, z) = r_e(L_B, 0) \times (1+z)^{-\frac{\eta}{p}(\frac{p}{\xi}-2.5)}, \quad (6)$$

which is a generalization of eq. 1.

The value of ξ depends on the physical process of mergers. Generally, merger products are expected to become more compact than pre-merger progenitors in gas-rich mergers because of efficient cooling and dissipation. On the other hand, merger products become less compact in gas-less mergers because the relative translational energy of pre-merger stellar progenitors is converted into the internal kinetic energy of a merged stellar system. The former corresponds to larger ξ , while the latter to smaller ξ . We use $\xi = 3$ as a standard value and examine the effect of changing this value. The assumed conservation of the total luminosity density of all galaxies (i.e., $\phi^*(z)L^*(z) = \text{constant}$) will also be discussed when we draw our conclusion of this paper.

2.5. Formulations

In the following we describe the formulations necessary to calculate the number count and redshift distribution of faint galaxies. We denote λ as the observed wavelength, and λ_D as the wavelength at which the object detection is performed. For example, we use $\lambda = \lambda_D = V_{606}$ or I_{814} for counts in the V_{606} and I_{814} bands, whereas $\lambda_D = I_{814}$ and $\lambda = U_{300}$ or B_{450} for the U_{300} and B_{450} bands (see §2.3.4).

The number of galaxies per unit steradian, per unit apparent magnitude (m_λ), and per unit redshift is written as

$$\frac{d^3N}{dm_\lambda dz d\Omega} = H(x) \frac{d^2V}{dz d\Omega} \sum_i \phi_i(M_B, z) \frac{dM_B}{dm_\lambda}, \quad (7)$$

where $x = D_{\lambda_D} - D_{\min}$, D_{λ_D} is the isophotal diameter of galaxies measured in the λ_D band, $d^2V/dzd\Omega$ is the comoving volume element which depends on the cosmological parameters, ϕ_i is the luminosity function per unit M_B with the Schechter parameters given in equation (3), and H is the step function [$H(x) = 1$ and 0 for $x \geq 0$ and < 0 , respectively]. The absolute B magnitude M_B is that of the present-day galaxies, which is related with z and m_λ by K -correction and evolutionary (E) correction (see equation 12 below). The subscript i denotes the galaxy type. The quantity $d^3N/dm_\lambda dz d\Omega$ gives the redshift distribution of galaxies, and the integration over z gives the number count or the number-magnitude relation.

We calculate D_{λ_D} and M_B as a function of m_λ and z , taking into account the selection effects and the photometry scheme. This is carried out as follows: For a given set of M_B and z , by using the assumed luminosity profile and the L_B - r_e relation, we first calculate the surface brightness distribution of a galaxy image in the λ_D band. Comparing this surface brightness distribution with the adopted threshold S_{th} in the λ_D band, we then calculate the isophotal diameter D_{λ_D} . Given this diameter, we calculate the isophotal magnitude in the λ band. (If the aperture magnitude is used in a survey, we should use the fixed aperture here. The pseudo-total magnitude is easily calculated simply from the total absolute magnitude without using the surface brightness distribution.) In this way we finally obtain m_λ as a function of M_B and z , or conversely M_B can be related to m_λ . It is obvious that D_{λ_D} is automatically obtained in this process. In the following we give detailed numerical formulations necessary for the above calculations.

Let $g(\beta)$ be radially symmetric luminosity profile (surface brightness distribution) of a galaxy, where $\beta = r/r_e$ is the radius from the center normalized by the effective radius of the galaxy. The adopted form of the profile is given by

$$g(\beta) = \exp(-a_n \beta^{1/n}), \quad (8)$$

and the integrated profile out to β is given by $G(\beta) \equiv 2\pi \int_0^\beta g(\beta') \beta' d\beta'$. We assume de Vaucouleurs' profile ($n = 4$) for elliptical galaxies and an exponential profile ($n = 1$) for spiral galaxies, as mentioned earlier. An effective radius r_e is defined as the radius within which a half of total luminosity is encircled, and by this definition the coefficient a_n is given by $a_4 = 7.67$ and $a_1 = 1.68$. In order to incorporate the effect of observational seeing, we convolve this profile function with a Gaussian PSF with dispersion σ_t :

$$\tilde{g}(\beta) = \int_0^\infty \frac{d\xi \xi}{\sigma_t^2} g(\xi) \left\{ I_0 \left(\frac{\beta \xi}{\sigma_t^2} \right) \exp \left(-\frac{\beta \xi}{\sigma_t^2} \right) \right\} \times \exp \left(-\frac{(\beta - \xi)^2}{2\sigma_t^2} \right), \quad (9)$$

where $I_0(x)$ is the modified Bessel function of the first kind

(e.g., Press et al. 1992). The seeing FWHM in units of radian is now related to σ_t as

$$\sigma_t = \left(\frac{\text{seeing FWHM}}{2.35} \right) \frac{d_A(z)}{r_e}, \quad (10)$$

where $d_A(z)$ is the standard angular diameter distance.

The surface brightness distribution of a galaxy image is given by

$$\begin{aligned} S_\lambda(\theta) [\text{mag arcsec}^{-2}] = & M_B + (\lambda - B)_0 + K_\lambda(z) + E_\lambda(z) \\ & + 2.5\tau_{\text{HI}}(\lambda, z) \log e \\ & + 5 \log[r_e(M_B, z)(1+z)^2/10\text{pc}] \\ & + 26.5721 \\ & - 2.5 \log[\tilde{g}(\beta)/G(\infty)], \end{aligned} \quad (11)$$

where θ is the angular radius from the center of a galaxy image, K_λ is the K -correction, E_λ is the E -correction including internal absorption by dust, and τ_{HI} is the optical depth of intergalactic absorption by HI clouds. The present-day color of galaxies of a given type, $(\lambda - B)_0$, is calculated by the AB colors based on the present-day SEDs of model galaxies which reproduce the observed colors, and we use $B_{450} - B = -0.153$ to relate the AB magnitudes to the B magnitudes of the luminosity function. The radius parameter β is related to θ as $\beta = d_A \theta / r_e$, and $G(\infty) = (2n)! \pi / a_n^{2n}$. The isophotal size D_{λ_D} can be derived from solving the equation $S_{\lambda_D}(D_{\lambda_D}/2) = S_{\text{th}}$. Similarly, the apparent magnitude encircled within θ is given by

$$\begin{aligned} m_\lambda(\theta) = & M_B + (\lambda - B)_0 + K_\lambda(\lambda, z) + E_\lambda(\lambda, z) \\ & + 2.5\tau_{\text{HI}}(\lambda, z) \log e + 5 \log[d_L/10\text{pc}] \\ & - 2.5 \log[\tilde{G}(\beta)/G(\infty)], \end{aligned} \quad (12)$$

where d_L is the standard luminosity distance, and $\tilde{G}(\beta)$ is the integrated profile of $\tilde{g}(\beta)$. The isophotal, aperture, and pseudo-total magnitudes are obtained with $\theta = D_{\lambda_D}/2$, aperture/2, and ∞ , respectively. (Note that $\tilde{G}(\infty) = G(\infty)$.)

The K and E corrections are calculated from the time-dependent models of spectral energy distribution per unit wavelength $f_\lambda(t)$, after modified to include the dust absorption. They can be written as

$$K_\lambda(z) = -2.5 \log \left\{ \frac{1}{(1+z)} \frac{f_{\lambda/(1+z)}(t_0)}{f_\lambda(t_0)} \right\}, \quad (13)$$

$$E_\lambda(z) = -2.5 \log \left\{ \frac{f_{\lambda/(1+z)}(t_z)}{f_{\lambda/(1+z)}(t_0)} \right\}, \quad (14)$$

where t_z is the age of a galaxy at redshift z which was formed at z_F , and t_0 is its present age.

With all these prescriptions, we can numerically solve M_B for a given set of m_λ and z , and then the number count and redshift distribution of galaxies by means of equation (7).

3. FAINT GALAXY NUMBER COUNTS

3.1. *Importance of the Observational Selection Effects*

Figure 5 shows the predictions of galaxy number count in the HDF based on the PLE model of galaxy evolution, including the effects of dust and intergalactic absorptions, and the selection effects. Here we have used a ‘standard’ set of model parameters in this paper: $(h, \Omega_0, \Omega_\Lambda) = (0.7, 0.2, 0.8)$, $z_F = 5$, the local luminosity function of the SSRS2 survey, and the screen model of dust. [Here, $h = H_0/(100\text{km/s/Mpc})$ as usual.] The solid line is the total number count of all galaxy types, and the other five lines are those of respective galaxy types. In this paper we will present many calculations of galaxy counts, changing various parameters in order to check the systematic uncertainties which may affect our conclusions. The summary of count calculations is presented in Table 2 with references to the number of figures in this paper.

In the following we compare these calculated counts with the HDF data as well as the ground-based data transformed into the AB magnitude system. Here we note that the HDF bandpass filters for the U_{300} and V_{606} are significantly different from those for the U , V , and R used in the ground-based observations. We have corrected the magnitudes of such ground-based data, making use of the central wavelength of bandpass filters, the present-day SEDs of different galaxy types, and the relative proportions among the galaxy types. The HDF counts are those of isophotal magnitudes, while published total-magnitude counts are used for other ground-based data for which the selection effects are not as important as for the HDF data.

Figure 6 shows the effect of cosmological parameters and the selection effects in the predictions of galaxy number count. The predictions with the selection effects are presented by solid lines, while those without the selection effects by dashed lines. In either cases, the three lines from bottom to top correspond to the EdS universe with $(h, \Omega_0, \Omega_\Lambda) = (0.5, 1, 0)$, an open universe with $(h, \Omega_0, \Omega_\Lambda) = (0.6, 0.2, 0)$, and a Λ -dominated flat universe with $(h, \Omega_0, \Omega_\Lambda) = (0.7, 0.2, 0.8)$.

The dotted line is a prediction without the selection effects in an open universe with $\Omega_0 = 0.1$. The prescriptions used here are the same as those in the prediction by Pozzetti et al. (1998) which they found to agree with the observed HDF counts. Our prediction shown by this dotted line also gives a good fit to the HDF data, and we have confirmed Pozzetti et al.’s result where no selection effects are taken into account. This suggests that the difference between the PLE models of different authors is not significant in the number count predictions.

However, this figure clearly demonstrates the importance of the selection effects in comparison between the predicted and observed number counts of galaxies. The

difference between the predicted counts with and without the selection effects attains up to a factor of about 4 at the faintest magnitudes. As a result, the observed HDF counts in excess of the PLE predictions with the selection effects are much larger than previously considered. It is striking that such PLE predictions seem to be short of the observed counts in all the passbands, even in the Λ -dominated flat universe with $\Omega_\Lambda = 0.8$ in which the number count is close to the maximum. In the EdS universe, such a predicted deficit in the PLE model attains up to a factor of more than 10. This large excessive number of HDF galaxies may suggest the number evolution of galaxies, but it depends heavily on the cosmology how much the number evolution is required to explain the HDF data.

3.2. *Dependence on Model Parameters*

Before we investigate the effect of number evolution quantitatively, it is necessary to see the uncertainties in the PLE predictions. Figure 7 shows how the PLE predictions depend on models of luminosity evolution and absorptions. The solid line is the standard model presented in Fig. 5. The dotted line is the same as the standard model but with no luminosity evolution. The dot-dashed line is the prediction where the updated luminosity evolution model of Kobayashi et al. (1999) is used rather than the standard model of Arimoto & Yoshii (1987) and Arimoto, Yoshii, & Takahara (1992). The short dashed line is the prediction where the slab distribution of dust is assumed rather than the screen by dust. The long-dashed line is the prediction where no intergalactic absorption is taken into account. This line almost overlaps with the solid line and is not visible except in the U_{300} band.

Figure 8 shows the effect of changing the galaxy formation epoch z_F and local luminosity function. The solid line is the standard model presented in Fig. 5. The short- and long-dot-dashed lines are the predictions with $z_F = 3$ and 10, respectively, rather than $z_F = 5$ in the standard model. The short- and long-dashed lines are the predictions where the luminosity function of the Stromlo-APM and the CfA redshift surveys are used, respectively, with $z_F = 5$.

Figure 9 shows how the uncertainty in the size-luminosity relation affects the predictions of galaxy number count. The solid line is the standard model presented in Fig. 5, while the dashed line is the prediction when the selection effects are ignored, as shown in Fig. 6. The short- and long-dot-dashed lines are the counts when the $r_e - L_B$ relation is shifted by $\pm 1\sigma$ in $\Delta(\log r_e)$. The dotted line is the prediction using the GCE sequence instead of the standard GDE sequence as the size-luminosity relation of elliptical galaxies. (See §2.3.1 for detail.)

From these three figures we understand a range of the systematic uncertainties in the PLE predictions, which turns out to be not large enough to save the EdS universe nor an open universe with $\Omega_0 > 0.2$. These uncer-

tainties are significant at the faintest magnitudes where the N - m relation starts to turn over. However, we point out that the effect of cosmological parameters becomes apparent at brighter magnitudes where the uncertainties remain much less significant. In fact, we will show that the slope of the N - m relation at $B_{450} = 22\text{--}26$ can be used to discriminate between the effects of cosmological parameters and galaxy number evolution. In order to demonstrate the above statement quantitatively, the systematic model uncertainties at $m = 25$ and 28 are summarized in Table 3. The uncertainty at $m = 25$, to be compared with the effect of cosmological parameters, is dominated by the dust distribution model, but we note that the estimated change from a standard screen model to the slab model is somewhat overestimated because the slab model is clearly inconsistent as a model of dust distribution in starburst galaxies, as mentioned in §2.2.

3.3. Mergers and Number Evolution

The PLE predictions fall considerably short of the observed HDF counts in the EdS universe and an open universe, and it is still the case even in a Λ -dominated flat universe. Here, by using a simple model of mergers introduced in §2.4, we investigate whether the number evolution explains the large number of faint HDF galaxies. Figure 10 shows the effect of introducing such a number evolution model in a Λ -dominated flat universe. The solid line is the prediction with the merger parameters of $(\eta, \xi) = (1, 3)$, while the dotted line is the standard PLE prediction with no number evolution (Fig. 5). The short- and long-dot-dashed lines are the predictions with $(\eta, \xi) = (1, 2)$ and $(1, 4)$, respectively, showing that the effect of changing ξ is not significant. This result indicates that a modest number evolution with $\eta \sim 1$ [$\phi^* \propto (1+z)^\eta$] is sufficient to explain the observed HDF counts in a Λ -dominated flat universe with $\Omega_\Lambda = 0.8$, and an even stronger number evolution with $\eta \gtrsim 1$ is rejected by the data.

Next we consider the EdS universe where the PLE count prediction is by more than one order of magnitudes smaller than those observed in the HDF (Fig. 11). The predictions with $\eta = 2, 3, 4$, and 5 are shown by four solid lines in order from bottom to top, with a fixed value of $\xi = 3$. The dotted line is the PLE prediction without number evolution. This result indicates that a strong number evolution with $\eta \gtrsim 3\text{--}4$ is necessary to explain the HDF counts in the EdS universe. We note that, while the strong number evolution explains the counts at the faintest magnitudes, it fails to explain the overall shape or slope of the N - m relation. This failure is clearly seen in the B_{450} band, where the strong number evolution makes the count slope less steep and deviate from the observations most prominently at $B_{450} = 22\text{--}26$. This argument is quite robust, because there should be an upper bound in the steepness of the N - m slope ($d \log N / dm < 0.4$), when the total luminosity density of all galaxies is conserved during the merger

process. In a more realistic case such as gas-rich mergers inducing starbursts, an even flatter slope is predicted, because galaxies before mergers are always fainter than those in the case of luminosity-density conservation. If one tries to explain the observed steep slope by mergers, it is necessary to contrive a merger process where galaxies before mergers are always brighter, in other words, the luminosity density of galaxies increases if the merger process is traced backwards—which we consider quite unrealistic. Therefore, we conclude that a strong number evolution in the EdS universe is unlikely to explain the observed counts over the whole range of apparent magnitudes.

Figure 12 shows the effect of introducing a number evolution model in an open universe with $\Omega_0 = 0.2$. The lines in this figure have the same meanings as in Fig. 11, but the four solid lines are the predictions with $\eta = 1, 2, 3$, and 4 in order from bottom to top. In this open universe, a number evolution with $\eta \gtrsim 2$ is necessary to explain the faintest counts, but again it can not explain the steep slope of the N - m relation in the B_{450} and V_{606} bands. This indicates that an open universe is also difficult to explain the HDF counts if $\Omega_0 > 0.2$. However, a lower-density open universe, for example, with $\Omega \sim 0.1$ might give a similar result with a Λ -dominated flat universe with $\Omega_0 = 0.2$ (see Fig. 6), and such an open universe could also explain the HDF counts if a modest number evolution of galaxies is taken into account.

4. PHOTOMETRIC REDSHIFT DISTRIBUTION

Although not as reliable as spectroscopic redshifts, photometric redshifts of galaxies are useful for statistical studies of high-redshift galaxies. Several groups have published catalogs of photometric redshifts for the HDF galaxies (e.g., Sawicki, Lin, & Yee 1997; Wang, Bahcall, & Turner 1998; Fernández-Soto, Lanzetta, & Yahil 1999). Here we compare our theoretical model with the photometric redshift distributions reaching $I_{814} = 28$ derived by Fernández-Soto et al. (1999), which utilizes not only the optical photometry of the HDF but also the information of the near-infrared J , H , and K bands. We have also compared our model with the other two catalogs of photometric redshifts by Sawicki et al. (1997) and Wang et al. (1998), and confirmed that the following result is hardly changed.

Figure 13 shows the observed redshift distribution in three I_{814} magnitude ranges. The model curves are our predicted redshift distributions of galaxies in a Λ -dominated flat universe with $\Omega_\Lambda = 0.8$. The area over which the models are calculated is chosen to coincide with the sky area covered by the observational analysis of Fernández-Soto et al. (1999): 5.31 arcmin^2 for $I_{814} < 26$ and 3.92 arcmin^2 for $I_{814} > 26$. Therefore, not only the shape but also the normalization of the predicted redshift distributions can be compared directly with the data. The

solid and dashed lines are the models with $(\eta, \xi) = (0, 3)$ and $(1, 3)$, respectively, with the selection effects taken into account. The dot-dashed line is the same as the dashed line with $(\eta, \xi) = (1, 3)$, but no selection effects are taken into account. It is clear that the selection effects give a bias against high-redshift galaxies, and this selection bias is significant especially at the faintest magnitudes. It is inevitable to include these effects when one uses the redshift distribution as a probe of number evolution of galaxies. Comparison with the data shows that a modest merger model with $\eta \sim 1$ in a Λ -dominated flat universe gives a reasonable fit to the photometric redshift distribution as well as galaxy counts, provided that the selection effects are properly taken into account.

Figure 14 compares the observed redshift distribution with the predictions in the EdS universe. The solid line is the prediction without number evolution, while other lines are those with $\eta = 3, 4$, and 5 with a fixed value of $\xi=3$. The selection effects are taken into account in all curves. A strong number evolution predicts that most of galaxies have lower redshifts of $z \lesssim 1$, deviating significantly from the observed distribution for $23 < I_{814} < 26$. If the assumption of conserved luminosity density is relaxed, the predicted distribution becomes peaked at an even lower redshift, because pre-merger galaxies in more realistic merger models are fainter than expected from the conserved luminosity density, as discussed in the previous section. This gives another argument that the EdS universe can not explain the observed number of HDF galaxies even if a strong merger is invoked, in addition to the argument in the previous section against the EdS universe based on the slope of the observed N - m relation.

Figure 15 is similar to Fig. 14, but for an open universe with $\Omega_0 = 0.2$. The predicted redshift distribution is still peaked at a lower redshift compared with the observed distribution. This discrepancy is significant for $23 < I_{814} < 26$, but not as serious as in the EdS universe.

5. DISCUSSION

In this paper we have shown that a strong number evolution with $\eta \gtrsim 3\text{--}4$ is necessary to explain the HDF counts at the faintest magnitudes in the EdS universe. The photometric redshift distribution of HDF galaxies suggests that a significant number of the faintest galaxies are at $z < 1$, and hence there must be a strong number evolution already operated at $z < 1$ to increase the number of galaxies by factor of about 10. Therefore, further argument for or against the EdS universe with strong number evolution of galaxies can be made from the observational constraints based on spectroscopic redshift surveys at $z < 1$.

Totani & Yoshii (1998) argued that such a strong number evolution at $z < 1$ is clearly inconsistent with the spectroscopic catalogs of galaxies reaching $z \sim 1$, at least for giant galaxies with $L \sim L^*$. This is based on a V/V_{\max} test for the galaxies in the Canada-France Redshift Sur-

vey (CFRS, Lilly et al. 1995), and an important finding is that the PLE model is not inconsistent with the spectroscopic data, giving a constraint on number evolution as $\eta = 1.8 \pm 0.7, 1.1 \pm 0.7$, and 0.5 ± 0.7 for the EdS universe, an open $\Omega_0 = 0.2$ universe, and a flat $\Omega_\Lambda = 0.8$ universe, respectively. Although the V/V_{\max} test favors a larger η in the EdS universe, this value seems smaller than that required to explain the HDF counts at the faintest magnitudes. These results have been confirmed for elliptical galaxies by Shade et al. (1999), in which they found that the population of massive early-type galaxies was largely in place by $z \sim 1$.

An independent constraint on galaxy mergers at $z < 1$ comes from statistical studies of merging galaxies inferred from high-resolution images. Recently, Le Févre et al. (2000) derived the evolution of merger rate from the HST images of the CFRS and LDSS galaxies. Their result suggests that L^* galaxies on the average have undergone about one merger event from $z = 1$ to 0, which corresponds to $\eta \sim 1$ and hence this is consistent with the number evolution in a Λ -dominated flat universe suggested by this paper.

Pozzetti et al. (1998) claimed that the PLE model can not explain all the observed data, although it well explains the HDF galaxy counts. The major discrepancies between the PLE model and the observed data were found in the evolution of the luminosity density in the universe. That is, the observed luminosity density increases more steeply to $z \sim 1$ than the PLE model prediction, and on the other hand, the PLE model predicts too high UV luminosity density at $3.5 < z < 4.5$ compared with the observation, because of intense starbursts in elliptical galaxies. However, Totani, Yoshii, & Sato (1997) had already pointed out that the observed steep evolution to $z \sim 1$ is explained in a Λ -dominated flat universe. It has already been argued that the PLE model is consistent with the observed luminosity density evolution if initial starbursts in high-redshift elliptical galaxies are obscured or not existent. In fact, our calculation of the redshift distribution in this paper shows that initial starbursts are not detected at $z \gtrsim 3$, because of the dust obscuration and the selection effects. Therefore, the major problems of the PLE model claimed by Pozzetti et al. (1998) are resolved, and the PLE model in a Λ -dominated flat universe gives a reasonable fit to the observed HDF data, allowing only for a modest number evolution of galaxies with $\eta \lesssim 1$.

6. SUMMARY AND CONCLUSIONS

We have modeled the number count and redshift distribution of faint HDF galaxies, with the observational selection effects properly taken into account. As a consequence of the selection effects in the theoretical modeling, predicted counts from the PLE model are smaller than previously considered, and they are more than 10 times

smaller than the observed HDF counts at the faintest magnitudes in the EdS universe. A strong number evolution with $\eta \gtrsim 3$ –4 under the assumption of conserved luminosity density is required to explain the faintest counts in this EdS universe, when the number evolution is parametrized as $\phi^* \propto (1+z)^\eta$ and $L^* \propto (1+z)^{-\eta}$. However, such a strong number evolution is not consistent with the overall N – m slope or the photometric redshift distribution. These discrepancies become even worse when one considers a more realistic merger process, i.e., enhanced star formation following by gas-rich mergers. In addition, such a strong evolution is rejected at least for average L^* galaxies at $z < 1$ from the data of spectroscopic redshift surveys (Totani & Yoshii 1998; Shade et al. 1999; Le Févre et al. 2000). Therefore, we conclude that it is almost impossible to explain the HDF galaxies in the EdS universe, unless we invoke ultra-exotic galaxy populations such as galaxies forming only massive stars at high redshifts to escape from local galaxy surveys due to the complete lack of long-lived stars.

The present work revitalizes the practice of using faint number counts as an important cosmological test, which gives one of the arguments against the EdS universe by its outstanding statistics compared with other cosmological tests. An open universe with $\Omega_0 > 0.2$ does not fit to the HDF data either, for the similar reasons for rejecting the EdS universe. An open universe with $\Omega_0 \sim 0.1$ might be consistent with the HDF data, but such a low value of $\Omega_0 \sim 0.1$ would not be reconciled with other constraints on Ω_0 , such as the baryon-gas to dark-matter mass ratio in poor clusters of galaxies combined with the standard big-bang nucleosynthesis prediction of baryon mass density in the universe (e.g., Pedersen, Yoshii, & Sommer-Larsen 1997).

We have extensively checked systematic uncertainties in our theoretical modeling of galaxy formation and evolution, and found that they are unlikely to resolve the above discrepancies emerged in the EdS universe and also in an open universe. On the other hand, such discrepancies are naturally resolved if we invoke a Λ -dominated flat universe. This suggests that the existence of the cosmological constant or an exotic form of the vacuum energy density of the universe which is now accelerating the expansion of the universe.

The PLE model in a Λ -dominated flat universe with $\Omega_0 \sim 0.2$ gives a reasonable fit to the HDF data, and a modest number evolution with $\eta \lesssim 1$ is also suggested by the HDF counts at the faintest magnitudes. It should

be noted that this number evolution does not necessarily mean mergers of galaxies, but may suggest strongly clumpy star-forming regions within an individual galaxy system becoming visible at high redshifts (Colley et al. 1996; Bunker, Spinrad, & Thompson 1999).

On the other hand, it is interesting to note that this indication of mild number evolution is consistent with the merger rate evolution of L^* galaxies at $z < 1$ recently inferred from a high-resolution image study for galaxies in the CFRS survey (Le Févre et al. 2000). This result is consistent with some models of galaxy formation based on the hierarchical structure formation in the CDM universe (Le Févre et al. 2000), although there are considerable uncertainties in the theoretical calculations for the merging history of baryonic component. A stronger number evolution with $\eta \gtrsim 1$ is, however, strongly disfavored by the observed HDF galaxy counts. This will give an important constraint when galaxy formation is modeled in the framework of the structure formation in a cold dark matter universe.

Inclusion of the selection effects in this paper leads to a considerably different result from previous studies on galaxy number count and redshift distribution. This means that any cosmological interpretations will be seriously misled if the selection effects are ignored. All future studies related to the detection and statistics of high-redshift galaxies should take into account these effects. The selection effects give a bias against high-redshift galaxies, reducing a problem of overprediction of such galaxies by the PLE model, which has been claimed by several studies ignoring the selection effects (e.g., Ellis 1997). In fact, we have shown that the PLE model is in overall agreement with the HDF galaxies, even if a modest number evolution of galaxies ($\eta \lesssim 1$) may be required. A strong number evolution, however, predicts too small a number of high-redshift galaxies to be consistent with the photometric redshift distribution of the HDF galaxies.

The authors would like to thank K. Shimasaku for providing numerical data for the filter functions of HST photometry bands, and T. Tsujimoto and C. Kobayashi for providing their models of galaxy evolution in a tabular form. We also thank an anonymous referee for many useful comments which have considerably improved this manuscript. This work has been supported in part by a Grand-in-Aid for Conter-of-Excellence Research (07CE2002) of the Ministry of Education, Science, and Culture in Japan.

REFERENCES

Arimoto, N., & Yoshii, Y. 1987, A&A, 173, 23
 Arimoto, N., Yoshii, Y., & Takahara, F., 1992, A&A, 253,
 21
 Bender, R., Burstein, D. & Faber, S.M. 1992, ApJ, 399,
 462
 Blumenthal, G., Faber, S., Primack, J. & Rees, M. 1984,
 Nature, 311, 517
 Bouwens, R., Broadhurst, T. & Silk, J. 1998, ApJ, 506,
 557

Bunker, A.J., Spinrad, H., & Thompson, R.I. 1999, submitted to AJ

Burstein, D. & Heiles, C. 1982, AJ, 87, 1165

Calzetti, D., Kinney, A.L., & Storchi-Bergmann 1994, ApJ, 429, 582

Colley, W.N., Rhoads, J.E., Ostriker, J.P., & Spergel, D.N. 1996, ApJ, 473, 63

de Vaucouleurs, G. 1962, in IAU symp. 15, Problems of Extragalactic Research, ed. G.C. MacVittie (New York: MacMillan), 3

Disney, M., Davies, J. & Phillips, S. 1989, MNRAS, 239, 939

Efstathiou, G., Ellis, R.S., & Peterson, B.A. 1988, MNRAS, 232, 431

Ellis, G.F.R., Sievers, A.W., & Perry, J.J. 1984, AJ, 89, 1124

Ellis, R.S. 1997, ARA&A, 35, 389

Fernández-Soto, A., Lanzetta, K.M., & Yahil, A. 1999, ApJ 513, 34

Freeman, K.C. 1970, ApJ, 160, 811

Fukugita, M., Takahara, F., Yamashita, K., & Yoshii, Y. 1990, ApJ, 361, L1

Gardner, J.P., Sharples, R.M., Carrasco, B.E., & Frenk, C.S. 1996, MNRAS, 282, L1

Hall, P. & Mackay, C.B. 1984, MNRAS 210, 979

Hatano, K., Branch, D., & Deaton, J. 1998, ApJ, 502, 177

Huchra, J.P., Davis, M., Latham, D. & Tonry, J. 1983, ApJS, 52, 89

Impey, C.D., Sprayberry, D., Irwin, M.J., & Bothun, G.D. 1996, ApJS, 105, 209

Jones, L.R., Fong, R., Shanks, T., Ellis, R.S. & Peterson, B.A. 1991, MNRAS 249, 481

Kobayashi, C., Tsujimoto, T., & Nomoto, K. 1999, submitted to ApJ, astro-ph/9908005

Kodama, T., & Arimoto, N., 1997, A&A, 320, 41

Koo, D.C. 1986, ApJ, 311, 651

Le Févre, O. et al. 2000, MNRAS, 311, 565

Lilly, S.J., Le Févre, O., Crampton, D., Hammer, F., & Tresse, L. 1995, ApJ, 455, 50

Loveday, J., Peterson, B.A., Efstathiou, G., & Maddox, S.J. 1992, ApJ, 390, 338

Madau, P. 1995, ApJ, 441, 18

Maddox, S.J., Sutherland, W.J., Efstathiou, G., Loveday, J., Peterson, B.A. 1990, MNRAS, 247, 1p

Marzke, R.O., Nicolaci da Costa, L., Pellegrini, P.S., Willmer, C.N.A., & Geller, M.J. 1998, ApJ, 503, 617

Metcalfe, N., Shanks, T., Fong, R. & Jones, L.R., 1991, MNRAS, 249, 498

Pei, Y.C. 1992, ApJ, 395, 130

Pedersen, K., Yoshii, Y., & Sommer-Larsen, J. 1997, ApJ, 485, L17

Pence, W. 1976, ApJ, 203, 39

Press, W.H. et al. 1992, Numerical Recipes, 2nd edition (Cambridge: Cambridge Univ. Press)

Pritchett, C. & Kline, M.I. 1981, AJ, 86, 1859

Pozzetti, L., Bruzual, G.A., & Zamorani, G. 1996, MNRAS, 281, 953

Pozzetti, L., Madau, P., Zamorani, G., Ferguson, H.C. & Bruzual, C.A. 1998, MNRAS 298, 1133

Rocca-Volmerange, B. & Guiderdoni, B. 1990, MNRAS, 247, 166

Sandage, A. 1961, ApJ, 133, 355

Sawicki, M.J., Lin, H. & Yee, H.K.C 1997, AJ, 113, 1

Schade, D. et al. 1999, ApJ, 525, 31

Schlegel, D., Finkbeiner, D., & Davis, M. 1998, ApJ, 500, 525

Spitzer, L., Jr. 1978, Physical Processes in the Interstellar Medium (New York: Wiley)

Tolman, R.C. 1934, Relativity, Thermodynamics, and Cosmology (Oxford: Clarendon Press)

Totani, T., Yoshii, Y. & Sato, K. 1997, ApJ, 483, L75

Totani, T. & Yoshii, Y. 1998, ApJ, 501, L177

Tyson, J.A. 1984, PASP, 96, 566

Tyson, J.A. 1988, AJ, 96, 1

Wang, Y., Bahcall, N., & Turner, E.L. 1998, ApJ 116, 2081

Williams, R.T. et al. 1996, AJ, 112, 1335

Yoshii, Y. 1993, ApJ, 403, 552

Yoshii, Y. & Fukugita, M. 1991, in Observational Tests of Cosmological Inflation, ed. T. Shanks et al. (Netherlands: Kluwer Academic Publisher), 267

Yoshii, Y. & Peterson, B.A. 1991, ApJ, 372, 8

Yoshii, Y. & Peterson, B.A. 1994, ApJ, 436, 551

Yoshii, Y. & Takahara, F. 1988, ApJ, 326, 1

Yoshii, Y. & Takahara, F. 1989, ApJ, 346, 28

TABLE 1
SCHECHTER PARAMETERS ADOPTED FOR LOCAL LUMINOSITY FUNCTIONS

Survey	Type	$\phi^* [\text{Mpc}^{-3}]$	α	M_B^*	References
SSRS2	E/S0	4.4×10^{-3}	-1.00	-19.37	1
	Sab–Scd	8.0×10^{-3}	-1.11	-19.43	
	Sdm	0.2×10^{-3}	-1.81	-19.78	
Stromlo-APM	All	1.4×10^{-2}	-0.97	-19.50	2
CfA	E/S0	4.6×10^{-3}	-0.88	-19.23	3
	Sab	3.8×10^{-3}	-1.00	-18.99	
	Sbc	6.6×10^{-3}	-0.44	-19.06	
	Scd	2.0×10^{-3}	-1.00	-19.34	
	Sdm	0.8×10^{-3}	-1.20	-19.29	

NOTE.— $H_0 = 100 \text{ km/s/Mpc}$. SSRS2 is adopted as a standard in our analysis. The value of M_B^* is given for the B band, which is related to B_{450} as $B_{450} = B - 0.153$.

REFERENCES.—(1) Marzke et al. (1998), (2) Loveday et al. (1992), (3) Huchra et al. (1983). See also Efstathiou, Ellis, & Peterson (1988) and Yoshii & Takahara (1989).

TABLE 2
FIGURE IDENTIFICATION FOR GALAXY COUNT CALCULATIONS

Examined Effects	Figure No.
Galaxy morphological types	5
Selection effects	6
Cosmological parameters	6
Galaxy luminosity evolution	7
Absorption (dust and intergalactic HI clouds)	7
Local luminosity function	8
Formation redshift z_F	8
Dispersion in the L_B - r_e relation	9
Merging of galaxies	10–12

TABLE 3
SENSITIVITY OF THE PREDICTED N - m RELATION TO THE CHANGE OF INPUT PARAMETERS

#	Change	U_{300}		B_{450}		V_{606}	
		$\Delta \log N_{25\text{mag}}$	$\Delta \log N_{28\text{mag}}$	$\Delta \log N_{25\text{mag}}$	$\Delta \log N_{28\text{mag}}$	$\Delta \log N_{25\text{mag}}$	$\Delta \log N_{28\text{mag}}$
1	Cosmology: $\Lambda \rightarrow \text{EdS}/\text{open}^a$	-0.227/-0.126	-0.513/-0.232	-0.446/-0.235	-0.610/-0.278	-0.493/-0.254	-0.601/-0.254
2	Evolution: AY, AYT \rightarrow KTN b	+0.048	-0.026	-0.027	-0.086	-0.056	-0.017
3	Dust absorption: screen \rightarrow slab	-0.085	-0.166	+0.062	+0.101	+0.137	+0.136
4	HI absorption: on \rightarrow off	+0.094	+0.138	+0.020	+0.009	+0.005	+0.008
5	Local LF: SSRS2 \rightarrow Stromlo-APM/CfA c	-0.119/+0.066	-0.283/-0.225	-0.071/+0.041	-0.218/-0.128	-0.042/+0.022	-0.187/-0.187
6	Formation epoch z_F : 5 \rightarrow 3/10	+0.054/-0.040	-0.101/+0.036	-0.070/-0.062	-0.151/+0.075	-0.119/-0.025	-0.151/+0.075
7	r_e - L_B relation: $+1\sigma/-1\sigma$ in $\Delta(\log r_e)^d$	-0.088/+0.045	-0.159/+0.103	-0.150/+0.069	-0.160/+0.098	-0.104/+0.050	-0.147/+0.050
Total systematic uncertainty e		± 0.157	± 0.339	± 0.155	± 0.277	± 0.185	± 0.275

^a Λ : $(\Omega_0, \Omega_\Lambda) = (0.2, 0.8)$, EdS: (1, 0), open: (0.2, 0)

^bAY: Arimoto & Yoshii (1987), AYT: Arimoto, Yoshii, & Takahara (1992), KTN: Kobayashi, Tsujimoto, & Nomoto (1999).

^cSee Table 1 for detail.

^dSee §2.3.1 for detail.

^eQuadratic sum of the rows 2, 3, 5–7. A mean value of the two numbers in the rows 5–7 is used in the sum.

NOTE.—The prescriptions of a standard model in our analysis include a Λ cosmology, AY-AYT evolution model, the local LF of SSRS2, $z_F = 5$, the screen model of dust absorption, and the intergalactic HI absorption.

[Complete version of this table is available at <http://th.nao.ac.jp/~totani/images/paper/ty2000-table3.ps>.]

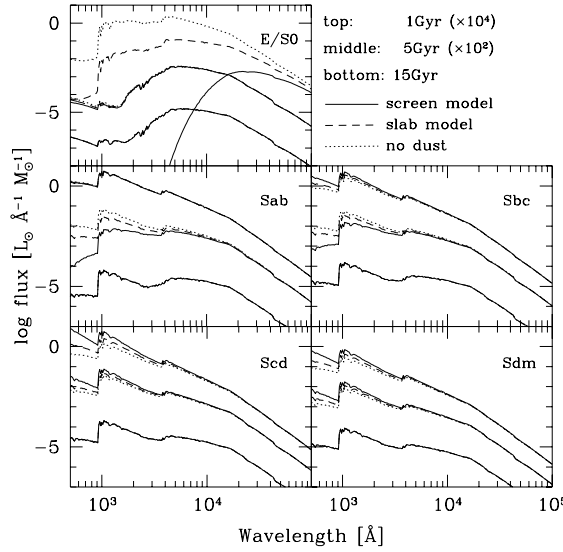


FIG. 1.— Spectral energy distributions (SEDs) of various morphological types of galaxies at epochs of 1, 5, and 15 Gyrs (from the top to the bottom) after their formation. For the purpose of clarity, the SEDs at 1 and 5 Gyrs are artificially multiplied by a factor of 10^4 and 10^2 , respectively. The screen model of dust extinction is used as our standard and is incorporated in the calculations shown by the solid line. The dashed and dotted lines are those from the slab dust model and the no-extinction model, respectively. The SEDs at 15 Gyrs are made to agree with the observed SEDs in the present-day galaxies.

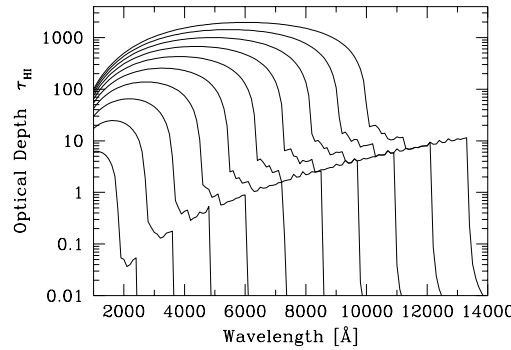


FIG. 2.— Optical depth of intergalactic absorption by intervening HI clouds as a function of observed wavelength for various source redshifts of $z = 1, 2, 3, \dots, 10$ (from left to right). Shown are the calculations by Yoshii & Peterson (1994), with the Doppler b -parameter of $b = 20$ km/s in the HI clouds (Spitzer 1978).

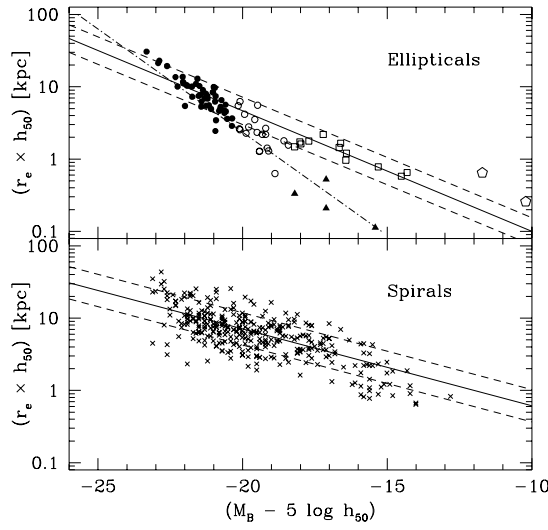


FIG. 3.— Size-luminosity relations for local elliptical and spiral galaxies. The data are from Bender et al. (1992) for elliptical galaxies and Impey et al. (1996) for spiral galaxies. For elliptical galaxies, the filled circles are for giant ellipticals, the open circles for intermediate ellipticals, the open squares for bright dwarf ellipticals, the filled triangles for compact ellipticals, and the open pentagons for dwarf spheroidals. The solid lines are the best-fit relations for the giant-dwarf elliptical sequence (GDE) and spiral galaxies, while the dot-dashed line is the best-fit to the giant-compact elliptical sequence (GCE). The dashed lines are the relation shifted by standard deviation in $\Delta(\log r_e)$ from the solid lines.

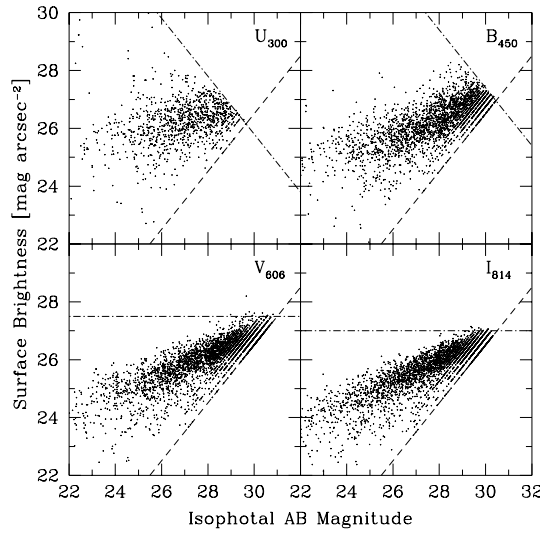


FIG. 4.— Isophotal AB magnitude versus average surface brightness of the HDF galaxies (Williams et al. 1996). The dashed line is the limit of minimum area of a galaxy image $A = 0.04 \text{ arcsec}^{-2}$. The dot-dashed lines in the V_{606} and I_{814} bands are the adopted isophotal thresholds ($S_{\text{th}} = 27.5$ and $27.0 \text{ mag arcsec}^{-2}$ for the V_{606} and I_{814} bands, respectively). The dot-dashed lines in the U_{300} and B_{450} bands correspond to the detection threshold by signal to noise ratio of $S/N > 2$ (see text).

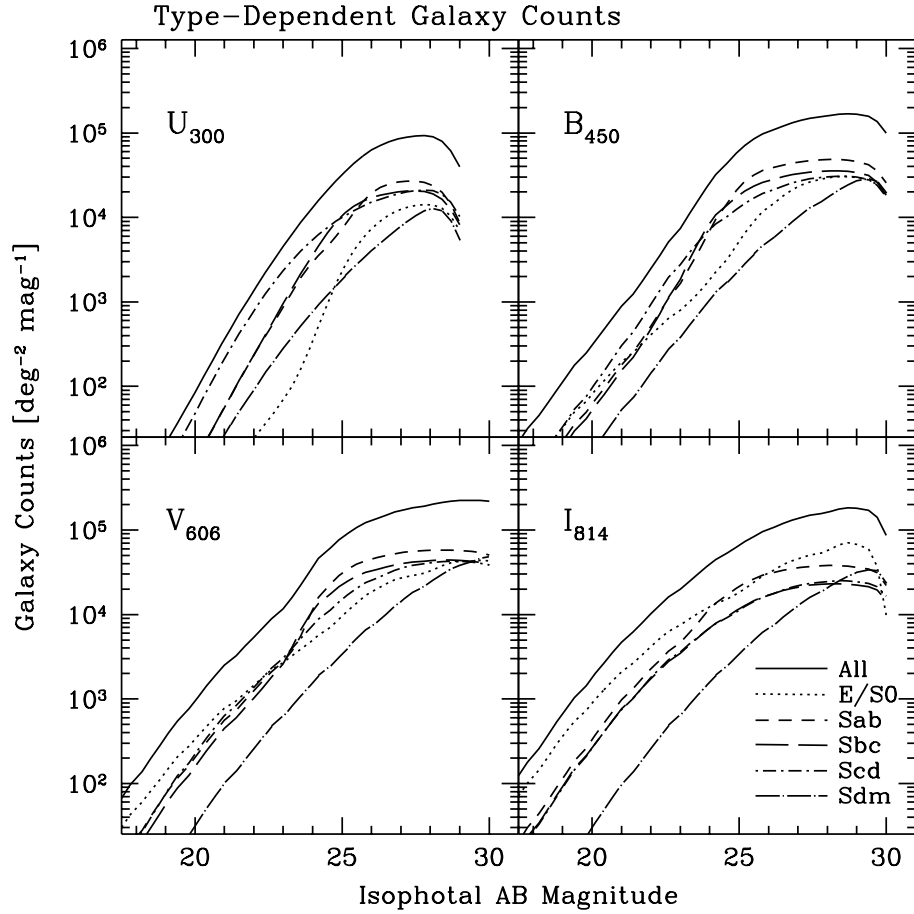


FIG. 5.— Faint galaxy number counts predicted in the four bands of the HDF. The selection effects under the HDF observation condition are included. The model presented here is our ‘standard’ PLE model with the standard set of model parameters: $(h, \Omega_0, \Omega_\Lambda) = (0.7, 0.2, 0.8)$, $z_F = 5$, the local luminosity function of the SSRS2 survey, and the screen model of dust extinction. Intergalactic absorption by HI clouds is also taken into account. The solid line is the total counts of all five types of galaxies, while the other lines are for individual types of E/S0 (dotted), Sab (short-dashed), Sbc (long-dashed), Scd (dot-short-dashed), and Sdm (dot-long-dashed).

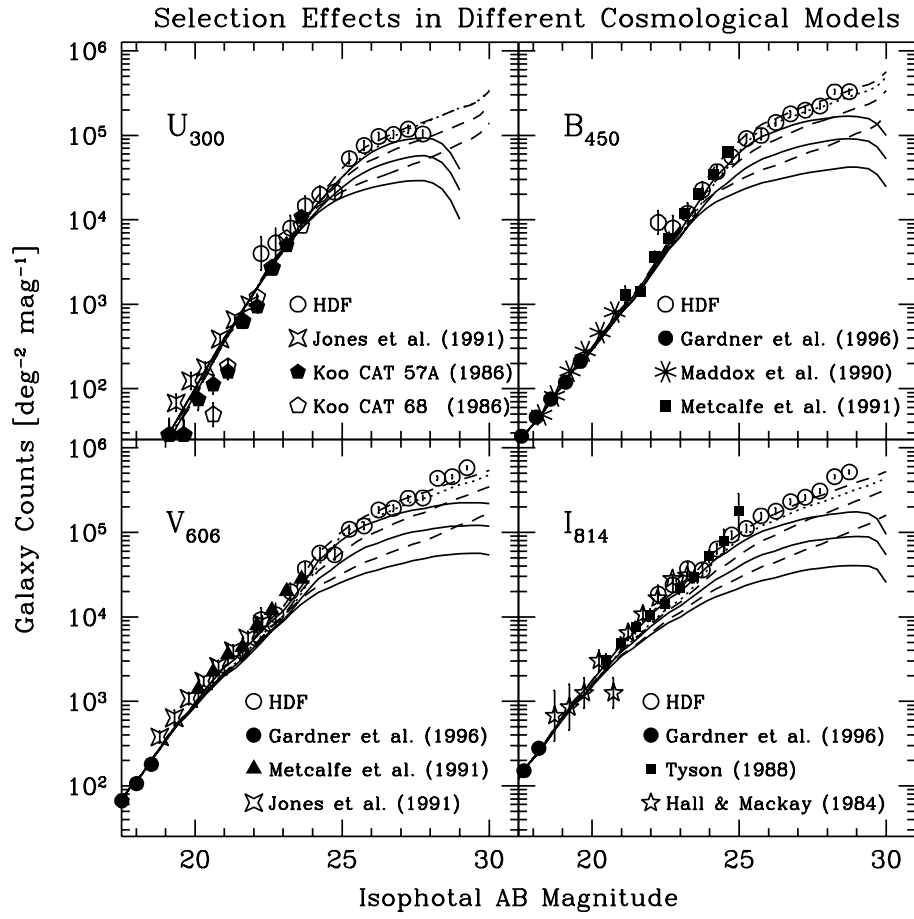


FIG. 6.— Comparison of the PLE model with the observed HDF counts as well as ground-based brighter counts. The top solid line is the standard PLE model shown in Fig. 5 in a Λ -dominated flat universe with $(h, \Omega_0, \Omega_\Lambda) = (0.7, 0.2, 0.8)$, while the middle and bottom lines are for the different cosmologies of an open universe with $(0.6, 0.2, 0.0)$ and an EdS universe with $(0.5, 1, 0)$, respectively. The three dashed lines from top to bottom are the same as the solid lines, except that the observational selection effects are not taken into account. The dotted line is a prediction in an open universe with $(h, \Omega_0, \Omega_\Lambda) = (0.6, 0.1, 0.0)$ and no selection effects, which are the same prescription with the previous study by Pozzetti et al. (1998).

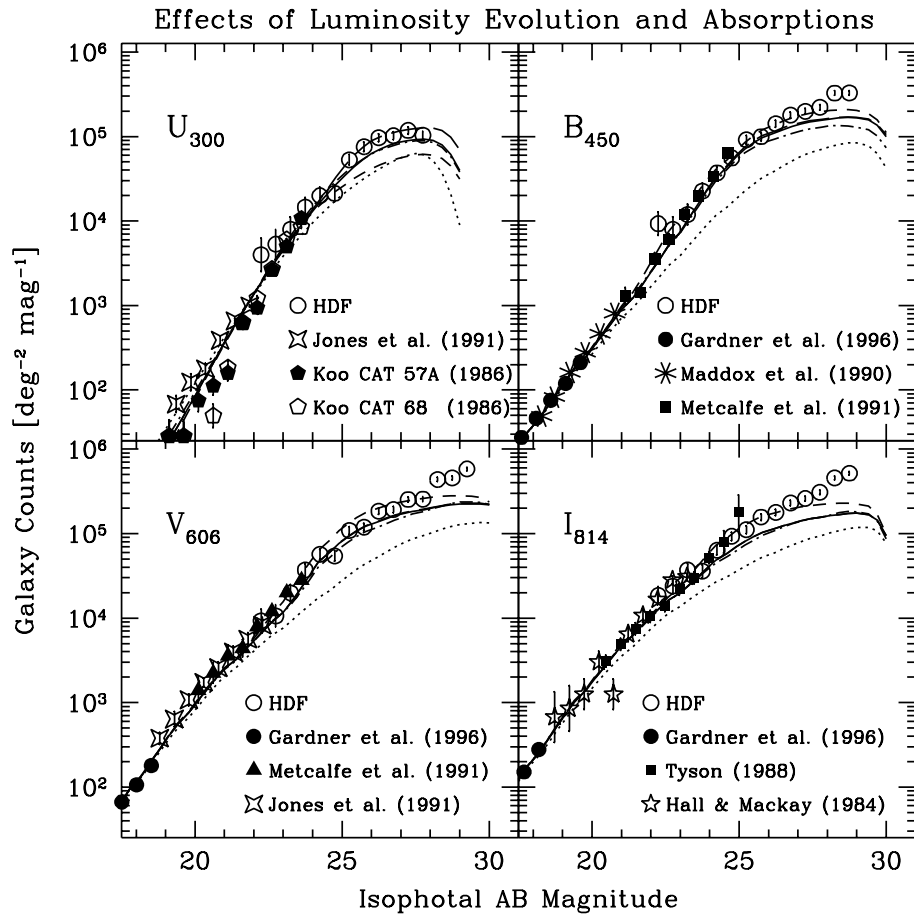


FIG. 7.— Comparison of the PLE model with the observed HDF counts as well as ground-based brighter counts. The solid line is the standard PLE model shown in Fig. 5. The other lines are the same but for the case of no luminosity evolution (dotted), slab model dust (short-dashed), no intergalactic absorption by HI clouds (long-dashed). The dot-dashed line is for the PLE model with the updated luminosity evolution model of Kobayashi et al. (1999).

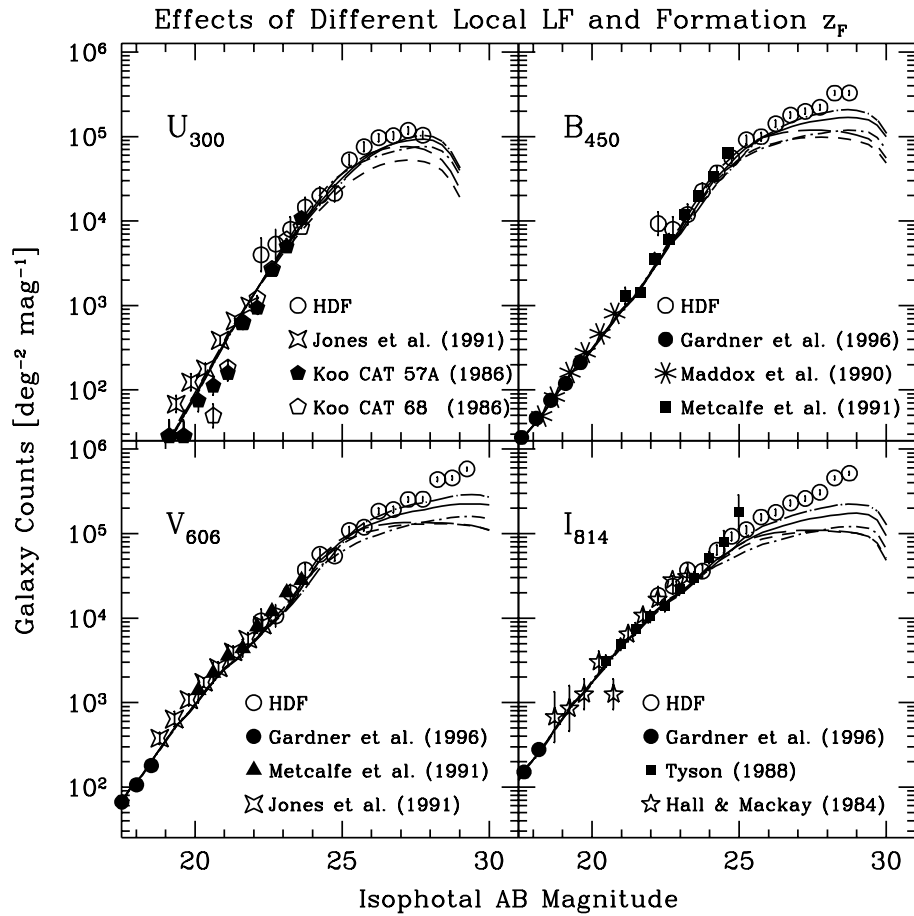


FIG. 8.— Comparison of the PLE model with the observed HDF counts as well as ground-based brighter counts. The solid line is the standard PLE model shown in Fig. 5. The other lines are the same but for the models with $z_F = 3$ (short-dot-dashed) and 10 (long-dot-dashed), and with different local luminosity functions of the Stromlo-APM survey (short-dashed) and the CfA survey (long-dashed).

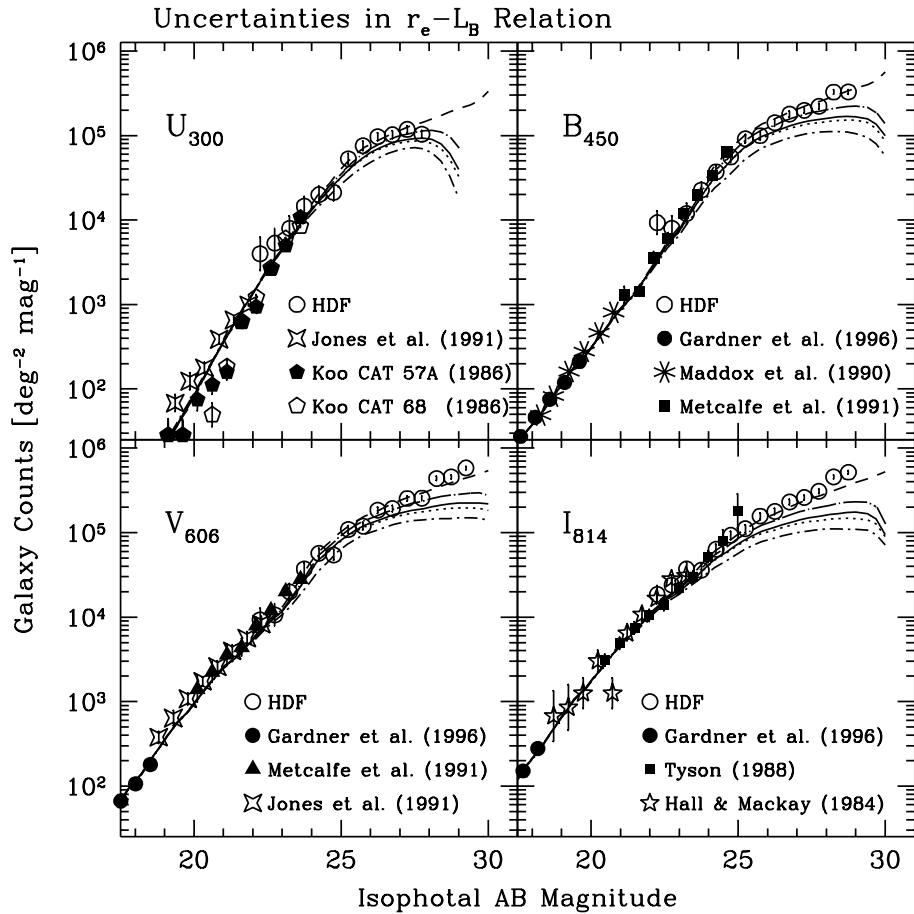


FIG. 9.— Comparison of the PLE model with the observed HDF counts as well as ground-based brighter counts. The solid line is the standard PLE model shown in Fig. 5. The other lines are the same but for models without the selection effects (dashed) and with the shifted size-luminosity relation by $+1\sigma$ (short-dot-dashed) and -1σ (long-dot-dashed) deviation in $\Delta(\log r_e)$. The dotted line is the PLE model where the GCE sequence of elliptical galaxies is used instead of the standard GDE sequence. See §2.3.1 for detail.

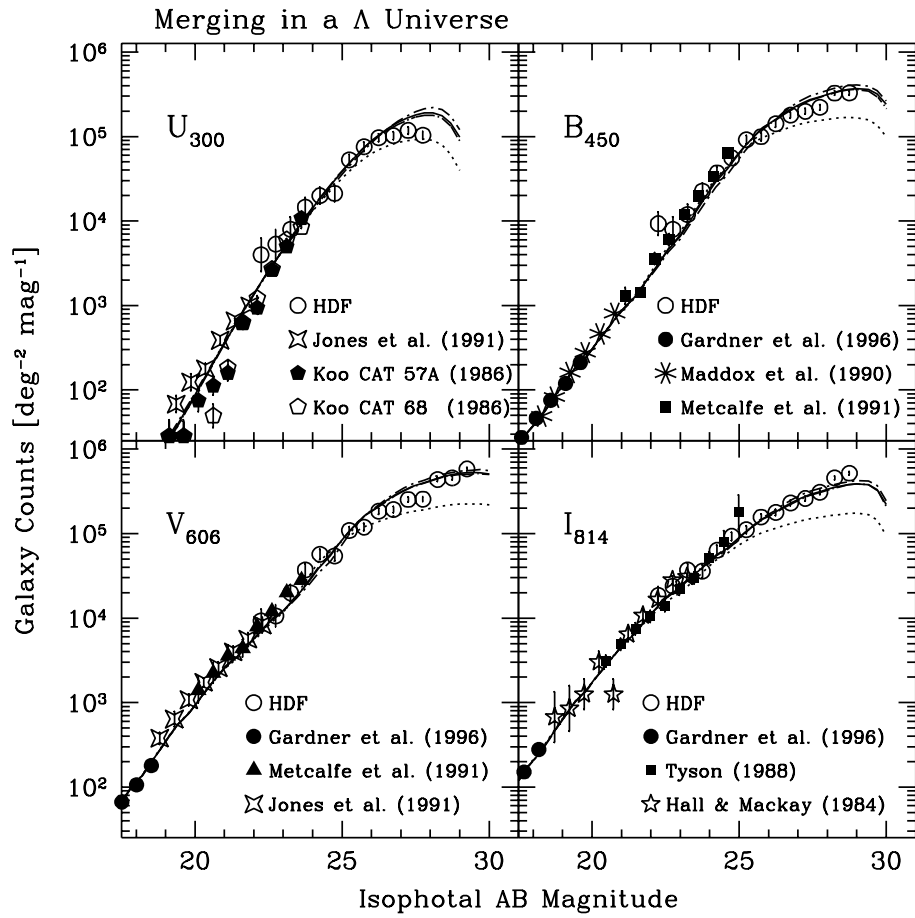


FIG. 10.— The effect of galaxy number evolution on galaxy counts based on the luminosity-density conserving mergers in a Λ -dominated universe with $(h, \Omega_0, \Omega_\Lambda) = (0.7, 0.2, 0.8)$. The dotted line is the standard PLE model without number evolution in this universe shown in Fig. 5 as well as Fig. 6. The short-dot-dashed, solid, and long-dot-dashed lines are the models with the merger parameters of $(\eta, \xi) = (1, 2)$, $(1, 3)$, and $(1, 4)$, respectively.

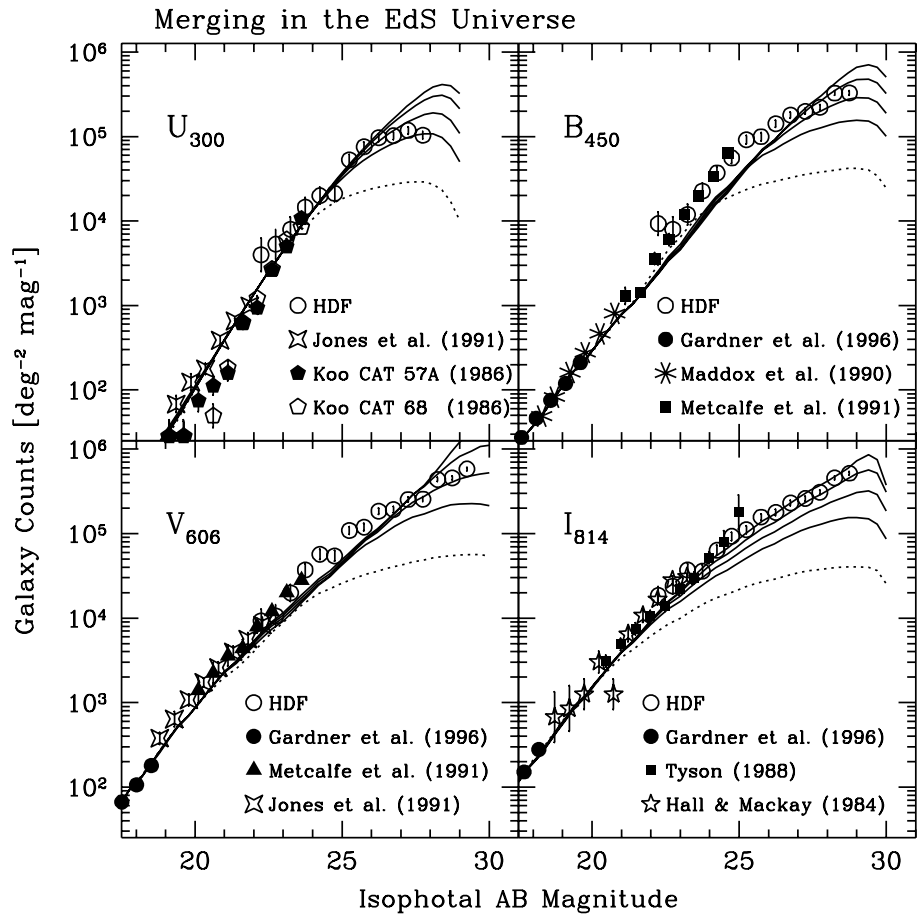


FIG. 11.— The effect of galaxy number evolution on galaxy counts based on the luminosity-density conserving mergers in the Einstein-de Sitter (EdS) universe with $(h, \Omega_0, \Omega_\Lambda) = (0.5, 1, 0)$. The dotted line is the standard PLE model without number evolution in the EdS universe shown in Fig. 6. The four solid lines are the models with the merger parameters of $\eta = 2, 3, 4$, and 5 (from the bottom to the top), where ξ is fixed to 3 .

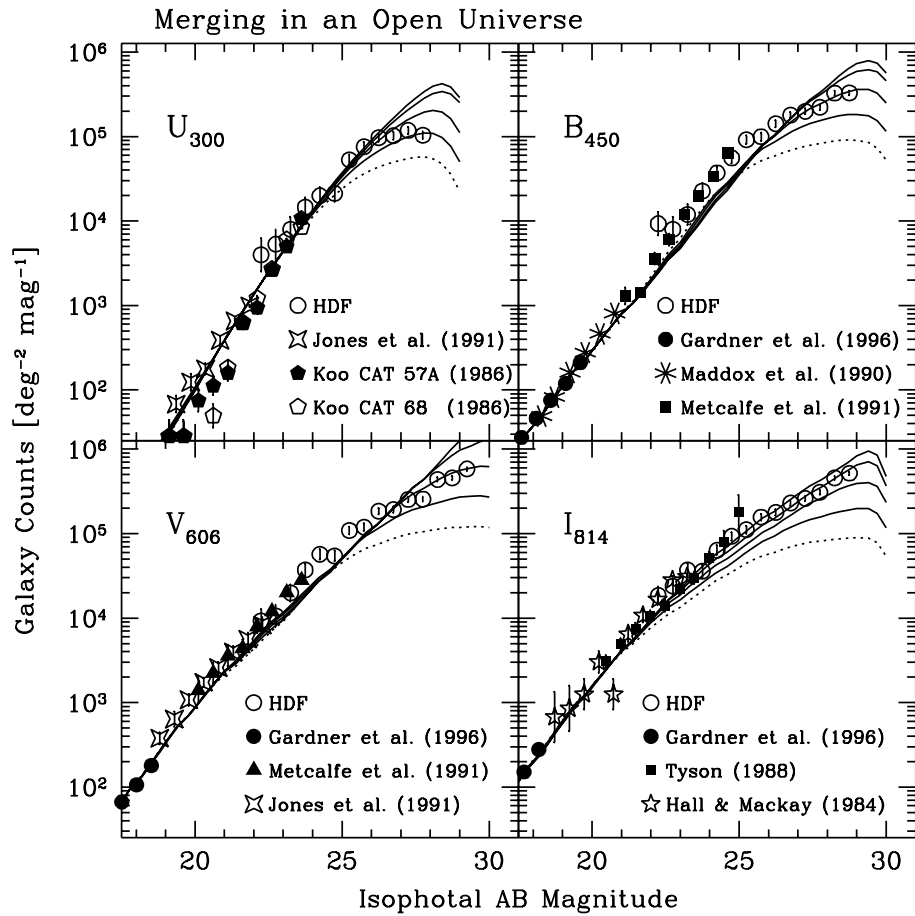


FIG. 12.— The effect of galaxy number evolution on galaxy counts based on luminosity-density conserving mergers in an open universe with $(h, \Omega_0, \Omega_\Lambda) = (0.6, 0.2, 0)$. The dotted line is the standard PLE model without number evolution in an open universe shown in Fig. 6. The four solid lines are the models with the merger parameters of $\eta = 1, 2, 3$, and 4 (from the bottom to the top), where ξ is fixed to 3.

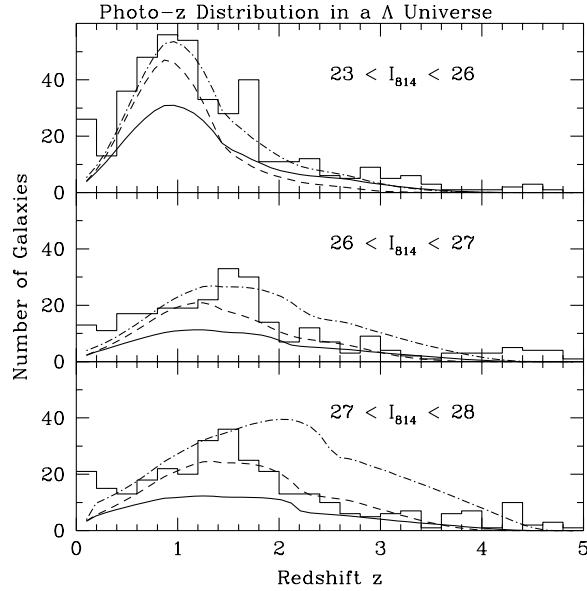


FIG. 13.— The comparison with the photometric redshift distribution derived by Fernández-Soto, Lanzetta, & Yahil (1999) in a Λ -dominated flat universe with $(h, \Omega_0, \Omega_\Lambda) = (0.7, 0.2, 0.8)$. The solid line is the standard PLE model without number evolution, with the same model parameters as in Fig. 5. The dashed line is the merger model with the merger parameters of $(\eta, \xi) = (1, 3)$, which reproduces the observed HDF number counts as well. The dot-dashed line is the same with the dashed line, but the selection effects are not taken into account.

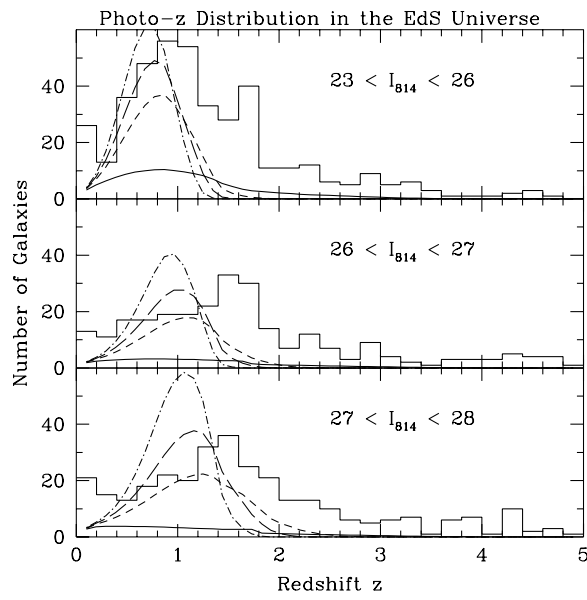


FIG. 14.— The comparison with the photometric redshift distributions derived by Fernández-Soto, Lanzetta, & Yahil (1999) in the Einstein-de Sitter universe with $(h, \Omega_0, \Omega_\Lambda) = (0.5, 1, 0)$. The solid line is the PLE model without number evolution. The short-dashed, long-dashed, and dot-dashed lines are the merger models with $\eta = 3, 4$, and 5 , respectively, where ξ is fixed to 3 . The selection effects are taken into account in all these models.

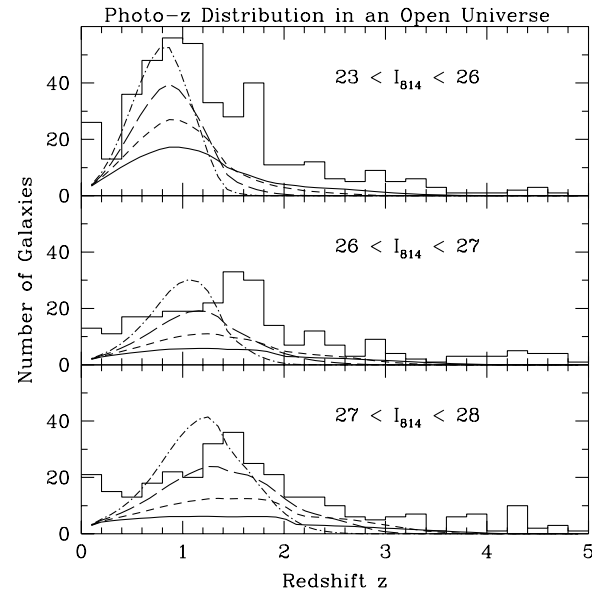


FIG. 15.— The comparison with the photometric redshift distributions derived by Fernández-Soto, Lanzetta, & Yahil (1999). The same as Fig. 14, but for an open universe with $(h, \Omega_0, \Omega_\Lambda) = (0.6, 0.2, 0)$. The solid line is the PLE model without number evolution. The short-dashed, long-dashed, and dot-dashed lines are the merger models with $\eta = 1, 2$, and 3 , respectively, where ξ is fixed to 3 . The selection effects are taken into account in all these models.